PCCP

PAPER

View Article Online
View Journal | View Issue

Tunability of hybridized plasmonic waveguide mediated by surface plasmon polaritons†

Cite this: *Phys. Chem. Chem. Phys.*, 2014, **16**, 16233

Ming-Ming Jiang,‡[a] Hong-Yu Chen,‡[ab] Chong-Xin Shan*[a] and De-Zhen Shen*[a]

Received 3rd April 2014,
Accepted 20th May 2014

DOI: 10.1039/c4cp01437e

www.rsc.org/pccp

Hybrid plasmonic waveguides have achieved rapid advancement in plasmonics, which has given rise to remarkable field enhancement, light harvest, light-transport capabilities, bridging the gap between electronics and photonics by routing and manipulating light at sub-wavelength regions and so on. However, the development of plasmonic waveguides is hindered by lack of devices that can adjust coherent plasmonic fields. In this letter, hybridized planar multilayer insulator metal insulator metal insulator heterostructures are proposed, and it is demonstrated that their unique capabilities can be used to adjust the mode characteristics by means of varying the thickness of the insulator spacer layer inserted between two metal films, such as the shift of the surface plasmon resonance wavelength. This type of hybrid plasmonic waveguides opens up opportunities for the tunability of mode characteristics, adjustment of resonant energy transfer processes, that have a potential for designing novel optical micro/nano resonance cavities.

1 Introduction

Plasmonics provides a route to develop ultracompact optical devices on a chip by using extreme light concentration and the ability to perform electrical and optical functions simultaneously. These properties make plasmonics an ideal candidate for dynamically adjusting photon–electron interactions at nanoscale.[1–5] These relatively novel devices are derived from manipulation of surface plasmon polaritons (SPPs)-electromagnetic waves which propagate along a metal surface, such as hybridized plasmonic waveguides, optical nano/micro cavities based on spasers.[6–9] One of the most remarkable characteristics associated with hybrid plasmonic waveguides generated from metal films or quasi-films (localized and propagating plasmons can also be supported by metallic quasi-films) at optical wavelengths, is the tunability of electronic collective oscillation.[10,11] Plasmonic waveguides can be applied to break through the diffraction limit, optical field imprisoned by means of dark modes *etc.*, such as surface enhanced Raman scattering, nanolasing, plasmonic sensing, and enhancement of spontaneous emission.[3,4,12,13] Plasmon lasers have been demonstrated theoretically[14] and experimentally[2,15] with silver (Ag) metal film and semiconductor materials. For instance, based on ZnO nanowire and Ag film, it is difficult to observe a deep sub-wavelength plasmonic laser action in the UV region.[2,3,16–21] The key to the problem may be the mismatch between the lasing of ZnO nanowire (~390 nm) with surface plasmon resonance based on hybrid plasmonic waveguide composed with Ag film.

The local surface plasmon resonance wavelength in metallic nanoparticles is highly dependent on the environment around the nanoparticles, as well as the coupling among the metal nanoparticles and the size of nanoparticles. An aggregation of metallic nanoparticles also exhibits a blue shift in the resonance wavelength changing from a red to a violet or a blue band, and for metal films as well.[22–25] If another metal film introduced to the plasmonic waveguide, the original waveguide would be transformed into a new kind of waveguide structure, such as metal–insulation–metal (MIM) waveguides. This new type of waveguide could exhibit oscillatory modes due to sufficient thickness of the intermediate dielectric core.[3,26–29] The coupling between surface plasmon polaritons at the two core/cladding interfaces changes significantly when the dielectric constants of the sub- and superstrates are different. The MIM waveguides can achieve extreme light concentration and manipulation, which help researchers distort nanophotonics space and mould the flow of light in an unprecedented fashion, which has been very widely used in perfect lens, hyperlens and transformation optics.[29–31] Additionally, MIM plasmonic waveguides can also be used to design novel plasmonic nano/micro-cavities, such as plasmonic Fabry–Perot resonant cavity. Such structures can quantize the energy of photons propagating along the optical axis of the cavity and thereby strongly modify the spontaneous emission properties of a photon-emitting medium inside a resonant cavity, metallic fins that reflect most of the incident surface plasmon to concentrate light within a sub-wavelength cavity mode. Therefore, metallic layers can

[a] *State Key Laboratory of Luminescence and Applications, Changchun Institute of Optics, Fine Mechanics and Physics, Chinese Academy of Sciences, No. 3888 Dongnanhu Road, Changchun, 130033, People's Republic of China. E-mail: shancx@ciomp.ac.cn, shendz@ciomp.ac.cn*

[b] *Graduate University of the Chinese Academy of Sciences, Beijing, 100049, People's Republic of China*

† Electronic supplementary information (ESI) available. See DOI: 10.1039/c4cp01437e

‡ These authors contributed equally to this work.

achieve much higher optical field confinement as well as sustaining a high Q-factor.[9,32,33] On-chip plasmon-induced transparency based on plasmonic coupled nanocavities can also be obtained due to the U-shaped plasmonic waveguide.[28]

Coupled surface plasmon polaritons (CSPPs) induced by double metal films construct plasmonic waveguides are reported to provide effective transfer of field enhancement from the surface of the upper metal film to the spacer (the space between the double layer metal film) on opposite sides of the upper metal films by means of controlling the spacer between two metal films.[4,34–36] The coupled SPPs happened in the spacer can be applied to achieve storage of electromagnetic energy, interspacer for electronic collective oscillation, photonic circuit integration, *etc*. Therefore, adjusting the coupling strength, tunability of plasmonic resonance and dark modes rapidly becomes an important factor for implementation of plasmonic circuit integration, microminiature plasmonic devices of light emitting diodes (LEDs), laser diodes (LDs) and biological sensing detectors.[12,37,38]

In this letter, a new kind of tunable hybrid plasmonic waveguide is considered by introducing another metal film accompanied with a low index dielectric layer between the present ones. For the insulation–metal–insulation–metal–insulation (IMIMI) hybrid plasmonic waveguide structures the red-shift of plasmonic resonance wavelength could be found from 450 to 600 nm, thereby achieving the tunability of hybrid plasmonic mode characteristics when a high-index dielectric nanowire is placed on the top surface of the IMIMI waveguides with a nanoscale gap. Plasmonic resonant energy transfer processes could be derived from the low-index dielectric spacer, as well as the tunability of mode characteristics. These tunable characteristics can be attributed to the coupling between the cylinder modes and hybrid plasmonic modes.

2 Tunability of hybridized plasmonic waveguides

On the basis of metal films adopted in plasmonic waveguide devices, the optical SPP waveguides are mainly classified into two categories, IMI-type and MIM-type.[39] If we take the IMIMI structure waveguide for example, $\varepsilon_1/\varepsilon_{m1}/\varepsilon_2/\varepsilon_{m2}/\varepsilon_3$, corresponding to the thickness of the layers d_1, d_{m1}, d_2, d_{m2}, d_3. Here ε_{m1} and ε_{m2} are the dielectric constants of the two different metal films, respectively, as shown in Fig. 1. Solving this system of linear equations results in an implicit expression for the dispersion relation linking β and ω *via*

$$e^{-2k_2d_2} = \frac{\left(1+\frac{\varepsilon_2k_{m2}}{\varepsilon_{m2}k_2}\right)\left(1+\frac{\varepsilon_{m2}k_3}{\varepsilon_3k_{m2}}\right)+\left(1-\frac{\varepsilon_2k_{m2}}{\varepsilon_{m2}k_2}\right)\left(1-\frac{\varepsilon_{m2}k_3}{\varepsilon_3k_{m2}}\right)e^{-2k_{m2}d_3}}{\left(1-\frac{\varepsilon_2k_{m2}}{\varepsilon_{m2}k_2}\right)\left(1+\frac{\varepsilon_{m2}k_3}{\varepsilon_3k_{m2}}\right)+\left(1+\frac{\varepsilon_2k_{m2}}{\varepsilon_{m2}k_2}\right)\left(1-\frac{\varepsilon_{m2}k_3}{\varepsilon_3k_{m2}}\right)e^{-2k_{m2}d_3}} \times \frac{\left(1-\frac{\varepsilon_1k_{m1}}{\varepsilon_{m1}k_1}\right)\left(1+\frac{\varepsilon_{m1}k_2}{\varepsilon_2k_{m1}}\right)+\left(1+\frac{\varepsilon_1k_{m1}}{\varepsilon_{m1}k_1}\right)\left(1-\frac{\varepsilon_{m1}k_1}{\varepsilon_1k_{m1}}\right)e^{-2k_{m1}d_{m1}}}{\left(1-\frac{\varepsilon_1k_{m1}}{\varepsilon_{m1}k_1}\right)\left(1-\frac{\varepsilon_{m1}k_2}{\varepsilon_2k_{m1}}\right)+\left(1+\frac{\varepsilon_1k_{m1}}{\varepsilon_{m1}k_1}\right)\left(1+\frac{\varepsilon_{m1}k_1}{\varepsilon_1k_{m1}}\right)e^{-2k_{m1}d_{m1}}},$$

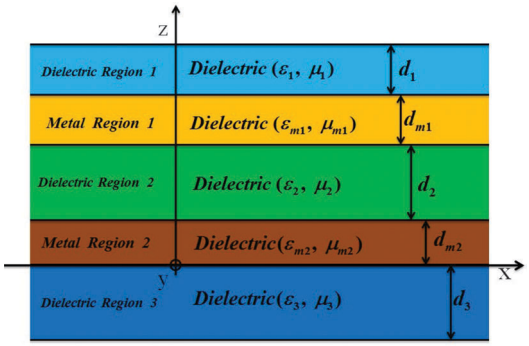

Fig. 1 Geometry of a five-layer system consisting of a IMIMI waveguide with permittivities $\varepsilon_1/\varepsilon_{m1}/\varepsilon_2/\varepsilon_{m2}/\varepsilon_3$, corresponding to the thickness of the layers d_1, d_{m1}, d_2, d_{m2}, d_3. Here ε_{m1} and ε_{m2} are the dielectric functions of the two different metal films, respectively.

and

$$k_{1(m1,2,m2,3)} = \sqrt{\beta^2 - \varepsilon_{1(m1,2,m2,3)}\frac{\omega^2}{c^2}} \quad (1)$$

According to the equation, the effective mode index of the surface plasmon polaritons for double metal films can be obtained, defined as $n_{eff} = \beta/k_0$, by varying the thickness of the second dielectric layer, d_2. When $d_2 \to 0$, the DSPP wave approaches the behavior of a DSPP wave for an $\varepsilon_1/\varepsilon_{m1}(\varepsilon_{m2})/\varepsilon_3$ structure; while d_2 is larger than the penetration depth of DSPP wave, the scenario is close to the DSPP wave for an $\varepsilon_1/\varepsilon_{m1}/\varepsilon_2$ structure. Based on the analysis, a tunable plasmonic waveguide was constructed, along with a high index nanowire placed on the upper metal film with a gap away from the metal layer. When d_2 is large enough, the mode is simplified as stated in previous reports.[14,15] There are three characteristic length scales involved when the surface plasmon wave is excited at the interface between the metal and dielectric films: propagation length of the SP mode δ_{SP}, decay length in the dielectric material δ_d, and decay length in the metal δ_m. In particular, δ_d is typically of the order of half the wavelength of light involved and establishes the maximum height of any individual features, and thus of the components that might be used to control the SPPs.[1] Therefore, when the gap distance is below a certain value, at the decay length δ_d excited in the dielectric material by the two layers of metal films, superposition states would appear, which results in splitting into symmetric and antisymmetric hybrid modes for the hybridized structures. The superposition of the decay wave occurring in the spacer can form coupling between the two metal films.[40,41]

2.1 Theoretical analysis of the tunable mode characteristics of a hybridized plasmonic waveguide

In order to theoretically understand the tunability of this kind of plasmonic waveguides, a novel hybrid plasmonic waveguide was proposed as shown in Fig. 2 consisting of a high-permittivity semiconductor nanowire (cylinder waveguide) embedded in a low-permittivity dielectric near the upper metal surface (double-surface plasmon polaritons (DSPP) waveguide)

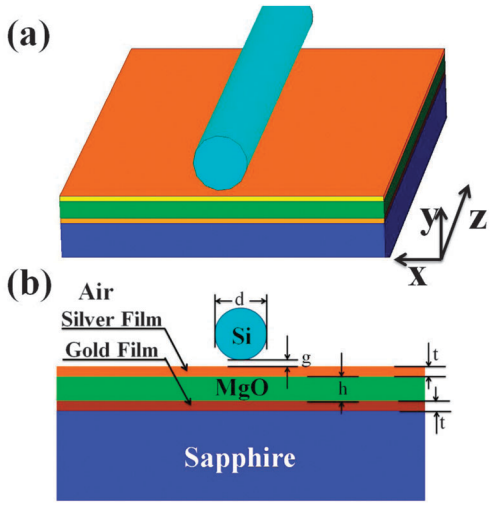

Fig. 2 Geometry of the tunable hybridized plasmonic waveguide: (a) schematic of the sample; (b) cross section of the hybridized plasmonic waveguide: a dielectric cylindrical nanowire with permittivity ε_c and diameter d is separated from the upper metallic half-space with permittivity ε_{m1} by a nanoscale dielectric gap with permittivity g and width t. The upper medium is a dielectric with permittivity ε_{d1}. The lower metallic half-space with permittivity ε_{m2}, the intermediate low index material permittivity h. ε_c = 12.25 (Si) and ε_{d1} = 2.25 (SiO_2), ε_{d2} = 2, $\varepsilon_{substrate}$ = 1.56, at a telecommunications wavelength λ_0 = 1.55 μm. The upper metallic region is silver with permittivity $\varepsilon_{m1} = -129 + 3.3i$, and the low metallic region is gold with permittivity $\varepsilon_{m1} = -110 + 10i$. The centre of the cylinder defines the origin ($x = y = 0$). The surrounding medium is set to be air (n_{air} = 1).

and there is another metal film, separated from the upper metal film with a distance h. An alternative method based on the coupled mode theory[14,15] was employed to describe the mode characteristics of the double metal films. The coupled mode theory applied to describe the mode hybridization of the three modes is referred to in the ESI.† Due to the geometry shown in Fig. 2, it could be found that the hybridized model has a cylinder-like mode and double metal films induced DSPP-like modes. The integrated model characteristic parameters could be described with the following three variables: diameter of the high-permittivity semiconductor nanowire d, gap distance between the high-permittivity semiconductor nanowire and the upper metal film g, gap distance between the double metal films h.

The thickness effect of the metal films is given in the ESI† shown in Fig. S5. When the thickness of metal film exceeds 30 nm, metal losses would prevent surface plasmon energy transfer. Therefore, the tunable mode characteristics of the hybridized plasmonic waveguide would disappear. On the contrary, when the thickness of metal films is too small, the mode characteristics will be uncontrollable. In particular, the silver and gold quasi-films were prepared in the experimental with a thickness of about 20 nm. For the sake of logic of this letter, the the thickness of metal films would be set to be 20 nm. The confinement of the electric field $E(x,y)$ the distribution in dielectric gap spacer region with d = 500 nm and g = 5 nm along y = 0 and x = 0 were calculated as shown in Fig. S2 (ESI†). It is demonstrated that when $g = h$ = 5 nm, the electromagnetic filed energy was mainly distributed in the dielectric spacer inserted double metal films shown in Fig. S2(a) (ESI†). Electromagnetic field $E(x,y)$ distribution would be transferred from the dielectric spacer to the gap area between the cylinder and the upper metal films when increasing the spacer thickness h, as shown in Fig. S2(b) (ESI†). The critical value of the spacer thickness for the energy storage area transfer is about 25 nm, which is very consistent with the shift of surface plasmon resonance wavelength derived from the change of dielectric spacer thickness.

The spacer thickness h is vital for the electromagnetic field energy distribution, as shown in Fig. 3. When the dielectric spacer thickness is very small, such as in the range of 5–15 nm, the electromagnetic field energy would be mainly concentrated

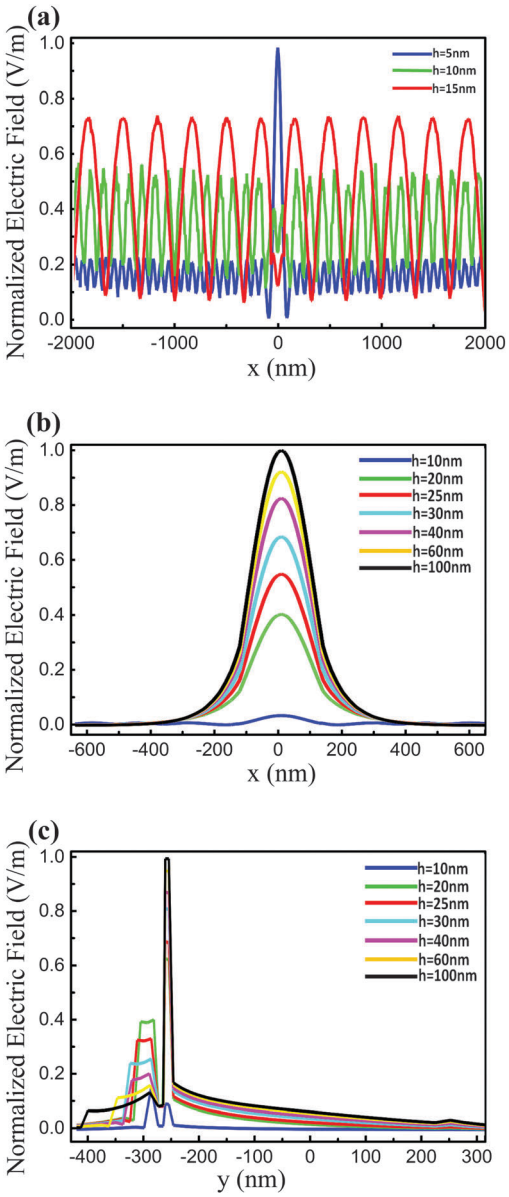

Fig. 3 (a) and (b) Confinement of the electric field $E(x,y)$ distribution in the dielectric gap spacer region with d = 500 nm, t = 20 nm and g = 5 nm along y = 0 with a variable spacer thickness h shown in the inset; (c) confinement of the electric field $E(x,y)$ distribution in the dielectric gap spacer region along x = 0 with a variable spacer thickness h.

in the dielectric spacer layer derived from Fig. 3(a). In particular, when $h = g = 5$ nm, the evanescent wave excited by the metal films can form coupling between the cylinder mode and the hybridized plasmonic mode with $t = 20$ nm. Therefore, a very prominent peak of electromagnetic filed energy distribution can be formed when the dielectric spacer thickness $h = 5$ nm. When further increasing the spacer thickness (such as more than 15 nm), the confinement of electromagnetic field would be transferred from the dielectric spacer region to the gap area between the cylinder and the upper metal film along $y = 0$ the transfer process detail can be referred to Fig. 3(b). The confinement of electric field $E(x,y)$ distribution in the dielectric gap spacer region along $x = 0$ demonstrated in Fig. 3(c) can be used as a proof for the shift of the electromagnetic field energy due to the variable spacer thickness h.

In order to gain further understanding of the transfer process, at moderate cylinder diameters ($d = 500$ nm), mode coupling results in a hybridized mode which features both cylinder and SPP characteristics; namely, its electromagnetic energy is distributed over both the cylinder and adjacent metal–dielectric interface (Fig. 4). However, when increasing the spacer thickness, the hybrid mode would display both the characteristics of a cylinder and a SPP mode. Interestingly though, it is strongly confined in two regions: within the gap between the cylinder and the upper metal film in the dielectric spacer with the two metal films inserted. Therefore, both in Fig. 3 and 4, the electromagnetic energy density distributions, as well as the transfer process can be expressed clearly with a variable spacer thickness h.

So as to form the hybridized modes consisting of a cylinder-like mode and DLSPP mode, the attention would be focused on the variable of the gap distance g between the cylinder and the upper metal film. Electromagnetic energy density distributions with $d = 500$ nm and $h = 75$ nm along $y = 0$ were calculated as shown in Fig. 5(a). The energy density along $y = 0$ shows sub-wavelength localization with variable g from 5 to 30 nm. However, when the gap distance exceeds 30 nm, the sub-wavelength localization with variable g will slowly disappear. The confinement of the electric field $E(x,y)$ distribution along $x = 0$ is displayed in Fig. 5(b). Evidently, the gap between the cylinder and upper metal film, and the dielectric spacer inserted between two metal films provide the means to store electromagnetic energy, leading to sub-wavelength optical guiding with low mode loss. This is further confirmed by resolving the electromagnetic energy density in more detail (Fig. 2, 3 and 5). Hence, the gap region and the spacer region can be treated as an area of low-permittivity dielectric directly beneath the cylinder and above the metal, and a low-permittivity dielectric directly inserted between two metal films. The strong energy confinement in the two regions occurs for two reasons. First, it arises from the continuity of the displacement field at the material interfaces, which leads to a strong normal electric-field component in the gap. Second, in both uncoupled SPP and cylinder geometries, the electric-field components normal to the material interfaces are dominant, amplifying the first effect. In fact, the dielectric discontinuity at the semiconductor–oxide interface produces a polarization charge that interacts with the plasma oscillations of the metal–oxide interface; that is, the gap region has an effective optical capacitance similar to that of a closely spaced metallic wire and plane.

As a result, for an arbitrary fixed thickness of the dielectric spacer layer, the gap distance g separated from the upper metal film of the MIM waveguide should be less than the spacer thickness, the hybrid plasmonic waveguides can provide sub-wavelength confinement by storing optical energy in the form

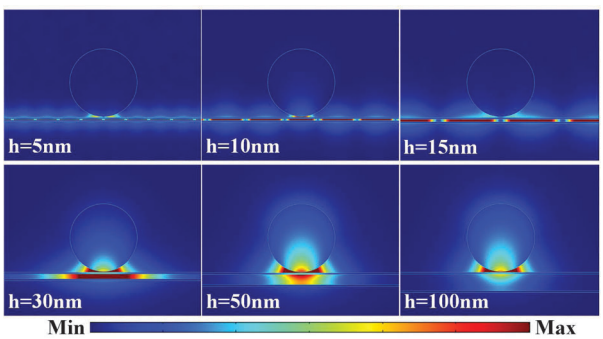

Fig. 4 Electromagnetic energy density distributions with a variable spacer thickness h, where $d = 500$ nm, $g = 5$ nm, and $t = 20$ nm.

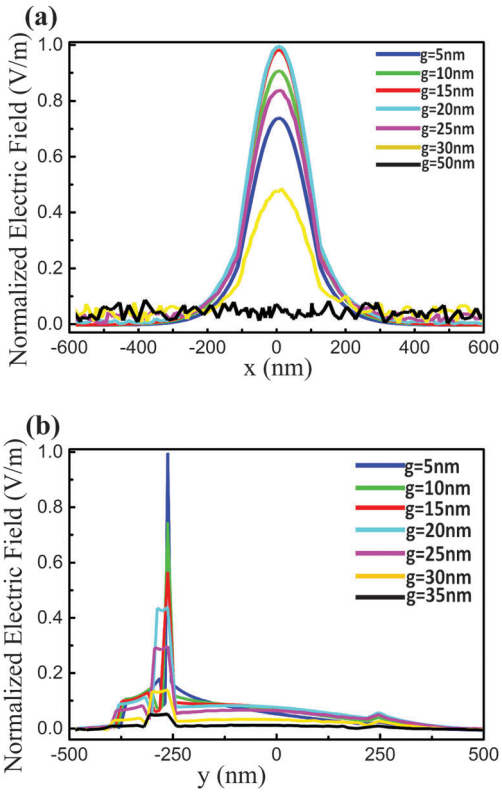

Fig. 5 (a) Confinement of the electric field $E(x,y)$ distribution with $d = 500$ nm and $h = 75$ nm along $y = 0$ with a variable gap distance between the cylinder and upper metal film g shown in the inset; (b) confinement of the electric field $E(x,y)$ distribution along $x = 0$ with a variable gap distance between the cylinder and upper metal film g shown in the inset, where the metal film thickness $t = 20$ nm.

of electron oscillations within dissipative metallic regions. When slowly increasing the spacer thickness h, the optical energy distribution will transfer from the dielectric spacer region with inserted two metal films to the gap between the cylinder and the adjustment metal film area. It is found that the dielectric spacer is capable of realizing the tunability of optical energy distribution by means of adjusting the spacer thickness of the inserted two metal films. The strong coupling between the dielectric cylinder mode and the DSPP mode supported at the interface of the dielectric environment capped cylinder and the MIM hybridized plasmonic waveguide results in an extremely confined hybrid plasmonic mode, while the evanescent coupling between the upper metal film mode and the low metal film coupling with the substrate act as perturbation to the hybrid mode, as elaborated below.

In order to further understand the mode characteristics of the hybrid mode, attention should be given to the tunability of mode characteristics, such as effective mode index, coupling strength, mode character and propagation distance.[14,39] The spacer thickness h was fixed to 75 nm (h = 50 nm and h = 100 nm can be found in the ESI†). According to the coupled mode theory calculated in the ESI,† the effective mode index $n_{hyb}(d,h)$, coupling strength $\kappa(d,h)$ between the cylinder-like mode and DSPP-like mode supported by the double metal films, the mode character $|a_+(d,h)|^2$ can be used to predict the transition between cylinder-like and SPP-like modes, and the propagation distance $L_m(d,h)$ is displayed in Fig. 6(a)–(d). Fig. 6(a) depicts the variation of the effective mode index. Naturally, in the limits of cylinder-like and SPP-like modes, the effective index approaches that of a pure cylinder, $n_{cyl}(d)$, or an SPP, n_{dspp} = 1.9 (h = 75 nm), mode. Compared with the results[14] n_{dspp} = 1.49, the difference is derived from the other metal film. When h = 50 nm, n_{dspp} = 2.14 and h = 100 nm, n_{dspp} = 1.83. Therefore, the spacer thickness h can be used to adjust n_{dspp}. The coupling strength gets its maximum value when $n_{cyl} = n_{dspp}$ at the critical diameter d_c of the cylinder waveguide, where the cylinder mode and DSPP mode propagate in phase and the effective optical capacitance of the coupled system is maximized, so that the coupling between the two modes is the strongest; so the mode character can predict the transition between cylinder-like and SPP-like modes. Variation of the spacer thickness does not only affect the critical diameter d_c of the cylinder waveguide changing from 330 to 280 nm, but also the coupling strength changes from 0.6 to 0.75 with h from 50 to 100 nm. The propagation distance L_m shown in Fig. 6(d) is also affected by the spacer thickness. The details and tunable mode characteristics of the hybridized plasmonic waveguides can be referred to in the ESI.†

A microminiature nanometer laser based on novel plasmonic devices and hybridized plasmonic waveguides helped overcome

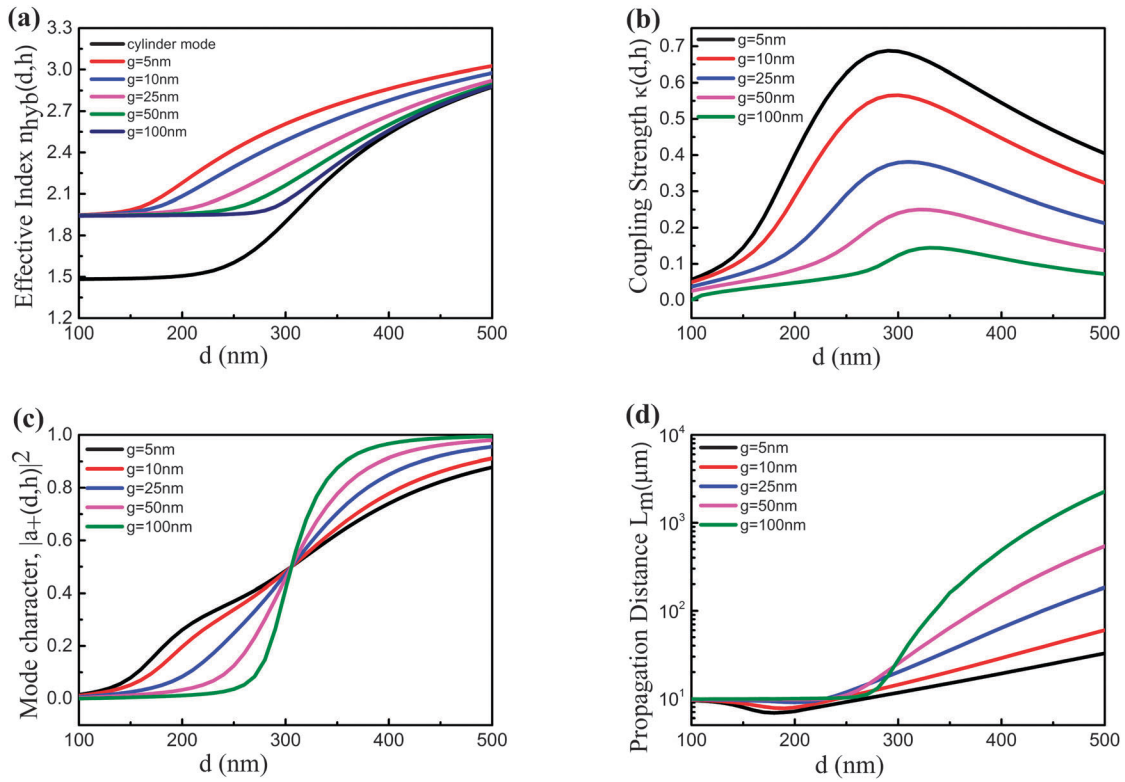

Fig. 6 Mode characteristics of a hybridized plasmonic waveguide: (a) mode effective index of the hybrid waveguide for a range of gap widths g and cylinder diameters d when h = 75 nm, the cylinder mode demonstrated shows a significant difference from the hybrid plasmonic modes induced by double metal films; (b) coupling strength $\kappa(d,h)$ dependent on the diameter of the cylinder and dielectric spacer thickness; (c) when $|a_+(d,h_1)|^2 > 0.5$ the mode is cylinder-like and $|a_+(d,h_1)|^2 < 0.5$, the mode is SPPs-like, hence, $|a_+(d,h_1)|^2 = 0.5$ means that maximum coupling occurs where the hybrid mode consists of equal proportions of cylinder and SPPs modes; (d) hybrid modes propagation distance L_m.

the challenge of the diffraction limit of light as a barrier limiting traditional optical components.[2,15,42,43] Metal films treated as a plasmon carrier, an electrical contact, and an effective heat sink have been successfully applied to study a plasmonic spaser, the design of plasmonic nanocavities and microcavities.[3,23,44] A further challenge is to achieve directional emission, which is difficult owing to the large momentum mismatch of photons emission and the surface plasmon resonance wavelengths. This kind of tunable hybridized plasmonic waveguide may provide new and creative approaches of efficient coupling of coherent nanoscopic light into a waveguide, which could route the light signals to various other devices such as detectors and modulators, as well as modulated plasmonic devices.[2,15,16,22,34]

2.2 Tunable surface plasmon resonances of the hybridized plasmonic waveguides

Graphene induced tunability of the surface plasmon resonance has been demonstrated by varying the thickness of an Al_2O_3 spacer layer inserted between graphene and the nanoparticles. By varying the spacer layer thickness from 0.3 to 1.8 nm, the resonance wavelength is shifted from 583 to 566 nm.[34] The gap inserted between these two films could provide a platform to achieve coupling between the surface plasmon wave excited by two layers of metal films. Due to the lack of broader regulation for the coupling derived from plasmonic guided modes by means of adjusting the spacer distance between two the metal films, the integration of plasmonic components based on tunable hybrid plasmonic waveguides restricts the development and applications of hybrid plasmonic waveguides.

In this letter, gold (99.99%) was first deposited on the c-face sapphire by a radio-frequency magnetron sputtering technique at room temperature with a pressure of 5×10^{-2} Pa, and subsequently annealed in a N_2 atmosphere at 350 °C to form a gold quasi-film. Then MgO thin film was deposited on the gold quasi-film by the MOCVD method, followed by silver (99.99%) quasi-film deposited on the MgO film with different thicknesses of the MgO film. By adjusting the MgO film thickness, a red-shift of plasmonic resonance wavelength from 450 to 600 nm was realized as shown in Fig. 7. The tunability of resonance wavelength of the local surface plasmon resonance (LSPR) by varying the distance between the gold quasi-film and silver quasi-film can be realized. It is estimated that every nanometer of change in the distance between two metal quasi-films corresponds to a resonance wavelength shift of ~7.5 nm. The gold and silver quasi-films separation changes the coupling strength of the electromagnetic field of the excited plasmons in the nanoparticles and the antiparallel image dipoles in the silver quasi-film.

Fig. 7 demonstrates that when the double metal films are prepared together directly, only the extinction spectra of gold can be observed at about 600 nm. But when the thickness of MgO layer between silver and gold films is increased, the plasmonic resonance wavelength will appear in a blue-shift. Once the thickness of the MgO layer exceeded 20 nm, the plasmonic resonance wavelength of the hybridized plasmonic

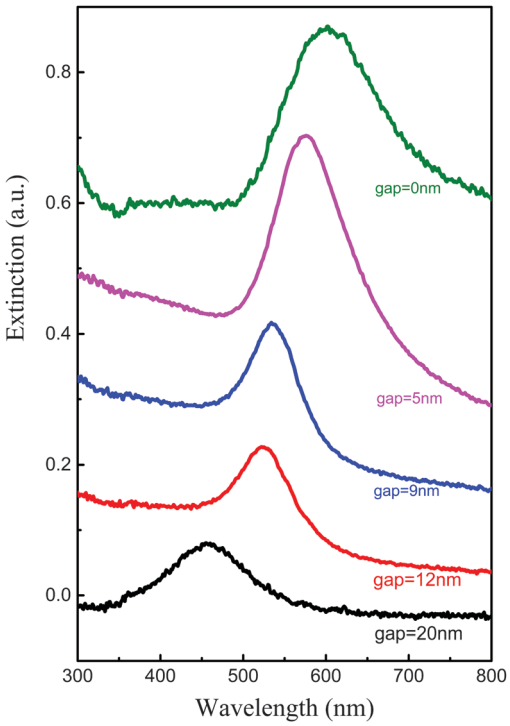

Fig. 7 Extinction spectra of two metal quasi-film mediated tunable surface plasmon resonances with different spacer layer gap, such as 0, 5, 9, 12, and 20 nm.

waveguide would stay at around 450 nm. These results are basically identical to our previous studies results of metal nanoparticles and single layer metal film surface plasmon resonance.[22,23] It can be found that by adjusting the thickness of the two kinds of metal films and the thickness of the dielectric layer sandwiched between them, the tunability of plasmonic resonance wavelength can be achieved. Meanwhile, tunability of the plasmonic resonance can also happen in the short wavelength range with Al metal films.[45]

The coupling strength between the evanescent waves excited by the metal quasi-films could be adjusted by means of adjusting the spacer thickness. Since the incident unpolarized light beam is perpendicular to the sample surface, the electric field has no vertical components with respect to the sample surface, which means only lateral electron oscillations in the metal films can be induced. When the spacer distance between double metal films is small, an antiparallel image dipole will be formed in the conducting film. The presence of an antiparallel image dipole will reduce the internal field in the metal films, which results in a red shift of the resonance wavelength, and the interaction between the dipoles will decrease as the spacer layer thickness increases. As a result, the resonance wavelength shows a blue shift with increasing the spacer layer. Therefore, our result implies the formation of laterally oscillating image dipoles in the Ag film. As proposed theoretically, the laterally oscillating image dipoles introduce a less resonance shift as compared to the vertically oscillating image dipoles. To induce the vertically oscillating image dipoles, an electric field with a component perpendicular to the sample surface must be presented.

For this purpose, the sample is tilted at various angles in our experimental setup and the transmission spectra are measured. But no additional resonance dip is observed and there is no observable change in the resonance wavelength as compared to the case of zero tilting, suggesting that no vertical oscillating dipole is present in our sample.[10,11]

3 Conclusion

The results given in this letter, could provide novel theoretical foundations for the tunability of a hybridized plasmonic waveguide which consists of a tunable low-index dielectric layer as a spacer. When the spacer thickness ranges from $\sim$5 to 30 nm, the surface plasmon resonance is red-shifted from 450 to 600 nm. Upon adjusting the spacer thickness, effective surface plasmon resonant energy transfer processes assisted plasmon hybridization processes can be realized, as well as energy transfer between the silver plasmon and gold plasmon. When a high-index dielectric semiconductor nanowire is placed on the upper metal film, the spacer layer inserted between the two metal films could achieve tunability of the mode characteristics of hybridized plasmonic waveguides, such as mode effective index, coupling strength, mode character, as well as the hybrid modes propagation distance. The IMIMI hybridized plasmonic systems approach based on plasmonic materials can represent a significant step towards novel applications of integrated plasmon-based circuitry, potential application of high gain, low threshold plasmonic amplifier and lasers based on different semiconductor nanowires in the future.

Acknowledgements

This work is supported by the National Basic Research Program of China (973 Program) under Grant Nos. (2011CB3020022011CB302004), the Key Program of the National Natural Science Foundation of China (11134009), the National Natural Science Foundation of China under Grant Nos. (21101146, 61177040) the 100 Talents Program of the Chinese Academy of Sciences.

References

1 W. L. Barnes, A. Dereux and T. W. Ebbesen, *Nature*, 2003, **424**, 824–830.
2 Y.-J. Lu, J. Kim, H.-Y. Chen, C. Wu, N. Dabidian, C. E. Sanders, C.-Y. Wang, M.-Y. Lu, B.-H. Li and X. Qiu, *et al.*, *Science*, 2012, **337**, 450–453.
3 K. Ding and C. Ning, *Light: Sci. Appl.*, 2012, **1**, e20.
4 C. Cirací, R. Hill, J. Mock, Y. Urzhumov, A. Fernández-Domínguez, S. Maier, J. Pendry, A. Chilkoti and D. Smith, *Science*, 2012, **337**, 1072–1074.
5 D. K. Gramotnev and S. I. Bozhevolnyi, *Nat. Photonics*, 2010, **4**, 83–91.
6 W. Cai, A. P. Vasudev and M. L. Brongersma, *Science*, 2011, **333**, 1720–1723.
7 M. Noginov, G. Zhu, A. Belgrave, R. Bakker, V. Shalaev, E. Narimanov, S. Stout, E. Herz, T. Suteewong and U. Wiesner, *Nature*, 2009, **460**, 1110–1112.
8 O. L. Berman, R. Y. Kezerashvili and Y. E. Lozovik, *Phys. Rev. B: Condens. Matter Mater. Phys.*, 2013, **88**, 235424.
9 B. Min, E. Ostby, V. Sorger, E. Ulin-Avila, L. Yang, X. Zhang and K. Vahala, *Nature*, 2009, **457**, 455–458.
10 T. Kelf, Y. Sugawara, R. Cole, J. Baumberg, M. Abdelsalam, S. Cintra, S. Mahajan, A. Russell and P. Bartlett, *Phys. Rev. B: Condens. Matter Mater. Phys.*, 2006, **74**, 245415.
11 M. Schwind, B. Kasemo and I. Zoric, *Nano Lett.*, 2013, **13**, 1743–1750.
12 Y.-H. Su, Y.-F. Ke, S.-L. Cai and Q.-Y. Yao, *Light: Sci. Appl.*, 2012, **1**, e14.
13 G. Lozano, D. J. Louwers, S. R. Rodríguez, S. Murai, O. T. Jansen, M. A. Verschuuren and J. G. Rivas, *Light: Sci. Appl.*, 2013, **2**, e66.
14 R. F. Oulton, V. J. Sorger, D. Genov, D. Pile and X. Zhang, *Nat. Photonics*, 2008, **2**, 496–500.
15 R. F. Oulton, V. J. Sorger, T. Zentgraf, R.-M. Ma, C. Gladden, L. Dai, G. Bartal and X. Zhang, *Nature*, 2009, **461**, 629–632.
16 V. J. Sorger, N. Pholchai, E. Cubukcu, R. F. Oulton, P. Kolchin, C. Borschel, M. Gnauck, C. Ronning and X. Zhang, *Nano Lett.*, 2011, **11**, 4907–4911.
17 M. A. Versteegh, D. Vanmaekelbergh and J. I. Dijkhuis, *Phys. Rev. Lett.*, 2012, **108**, 157402.
18 S. Chu, G. Wang, W. Zhou, Y. Lin, L. Chernyak, J. Zhao, J. Kong, L. Li, J. Ren and J. Liu, *Nat. Nanotechnol.*, 2011, **6**, 506–510.
19 D. Vanmaekelbergh and L. K. van Vugt, *Nanoscale*, 2011, **3**, 2783–2800.
20 S. Rodriguez, S. Murai, M. Verschuuren and J. G. Rivas, *Phys. Rev. Lett.*, 2012, **109**, 166803.
21 S. Thongrattanasiri and F. J. G. de Abajo, *Phys. Rev. Lett.*, 2013, **110**, 187401.
22 M.-M. Jiang, H.-Y. Chen, B.-H. Li, K.-W. Liu, C.-X. Shan and D.-Z. Shen, *J. Mater. Chem. C*, 2013, **2**, 56–63.
23 M.-M. Jiang, B. Zhao, H.-Y. Chen, D.-X. Zhao, C.-X. Shan and D.-Z. Shen, *Nanoscale*, 2014, **6**, 1354–1361.
24 P. Andrew and W. Barnes, *Science*, 2004, **306**, 1002–1005.
25 Y.-K. Liu, S.-C. Wang, Y.-Y. Li, L.-Y. Song, X.-S. Xie, M.-N. Feng, Z.-M. Xiao, S.-Z. Deng, J.-Y. Zhou and J.-T. Li, *et al.*, *Light: Sci. Appl.*, 2013, **2**, e52.
26 S. Feng, X. Zhang and P. J. Klar, *Appl. Phys. Lett.*, 2011, **99**, 053119.
27 Z. Ye, Y. Peng, T. Zhai, Y. Zhou and D. Liu, *J. Opt. Soc. Am. B*, 2011, **28**, 502–507.
28 Y. Zhu, X. Hu, H. Yang and Q. Gong, *Sci. Rep.*, 2014, **4**, 3752.
29 J. A. Schuller, E. S. Barnard, W. Cai, Y. C. Jun, J. S. White and M. L. Brongersma, *Nat. Mater.*, 2010, **9**, 193–204.
30 A. Vakil and N. Engheta, *Science*, 2011, **332**, 1291–1294.
31 J. B. Pendry, *Phys. Rev. Lett.*, 2000, **85**, 3966.
32 S.-W. Chang, T.-R. Lin and S. L. Chuang, *Opt. Express*, 2010, **18**, 15039–15053.
33 V. J. Sorger, R. F. Oulton, J. Yao, G. Bartal and X. Zhang, *Nano Lett.*, 2009, **9**, 3489–3493.

34 J. Niu, Y. Jun Shin, Y. Lee, J.-H. Ahn and H. Yang, *Appl. Phys. Lett.*, 2012, **100**, 061116.
35 A. González-Tudela, P. Huidobro, L. Martn-Moreno, C. Tejedor and F. Garca-Vidal, *Phys. Rev. Lett.*, 2013, **110**, 126801.
36 H. Noh, Y. Chong, A. D. Stone and H. Cao, *Phys. Rev. Lett.*, 2012, **108**, 186805.
37 B. Peng, Q. Zhang, X. Liu, Y. Ji, H. V. Demir, C. H. A. Huan, T. C. Sum and Q. Xiong, *ACS Nano*, 2012, **6**, 6250–6259.
38 Y. Gu, S. Xu, H. Li, S. Wang, M. Cong, J. R. Lombardi and W. Xu, *J. Phys. Chem. Lett.*, 2013, **4**, 3153–3157.
39 S. A. Maier, *Plasmonics: Fundamentals and Applications*, Springer, 2007.
40 B. Wang, X. Zhang, F. J. Garca-Vidal, X. Yuan and J. Teng, *Phys. Rev. Lett.*, 2012, **109**, 073901.
41 F. Schertz, M. Schmelzeisen, M. Kreiter, H.-J. Elmers and G. Schönhense, *Phys. Rev. Lett.*, 2012, **108**, 237602.
42 V. J. Sorger and X. Zhang, *Science*, 2011, **333**, 709–710.
43 X. Shan, U. Patel, S. Wang, R. Iglesias and N. Tao, *Science*, 2010, **327**, 1363–1366.
44 M. T. Hill, M. Marell, E. S. Leong, B. Smalbrugge, Y. Zhu, M. Sun, P. J. van Veldhoven, E. J. Geluk, F. Karouta and Y.-S. Oei, *et al.*, *Opt. Express*, 2009, **17**, 11107–11112.
45 M. W. Knight, N. S. King, L. Liu, H. O. Everitt, P. Nordlander and N. J. Halas, *ACS Nano*, 2013, **8**, 834–840.

